ADVANCED OPTICAL MATERIALS
www.advopticalmat.de

Ecofriendly Perovskites with Giant Self-Defocusing Optical Response

Isaac Suárez, Juan P. Martínez-Pastor, Marek F. Oszajca, Norman A. Lüchinger, Brian Graves, Said Agouram, Carles Milián, and Albert Ferrando**

The full optical control of light using sustainable green technologies is one of the incipient challenges of the Photonics community. There are, however, few optical materials able to provide a significant nonlinear refractive index change under small enough intensities (< 1 GW cm^{-2}), and, more importantly, allowing the external control of the magnitude and sign of their nonlinear response. This manuscript demonstrates that Cs_2SnI_6 lead-free nanocrystals (NCs) present an extraordinary self-defocusing response not yet observed up to now in any material. Despite its complex structural form, these NCs are fully characterized here, both experimentally and theoretically, revealing a giant negative refractive change $\Delta n = -0.05$ under proper illumination conditions. The nonlinear response is tuned with the intensity, concentration of NCs in the solvent, and propagation distance leading to a crossover where the media transforms to self-focusing with $\Delta n = +0.002$. These results can provide fascinating opportunities in sensing and light–matter interactions for a future ecofriendly photonic technology.

1. Introduction

The active optical control of the matter represents one of the ultimate goals of Photonics, with fascinating opportunities in optical signal processing, optical switching, light-induced metastability, or other disruptive applications.[1] The ability to engineer the refractive index of a given medium will influence the intensity, phase, and polarization of the incident light.[2] In particular, the nonlinear susceptibility (χ^{NL}) of the material determines the sign and magnitude of the light intensity (I) dependent, refractive index change, $\Delta n(I)$, and with it, the perspective to observe a rich variety of phenomena. Well-known examples include harmonic and supercontinuum generation, saturable absorption, or frequency combs.[3] Moreover, even more vanguardist applications can be demonstrated with $\Delta n < 0$. In that case, the material presents a self-defocusing response that can be exploited in polariton condensates,[4] shock waves,[5] or dark solitons.[6] However, in most materials χ^{NL} is so small that the required Δn for practical applications is either prevented or only manifested under extreme light intensities. For example, the typical nonlinear coefficient of Si or III–V semiconductors below the bandgap is 10^{-5} cm^2 GW^{-1},[7] which leads to a moderate $\Delta n = 10^{-5}$ with an intensity of 1 GW cm^{-2}. Indeed, it is particularly difficult to observe a self-defocusing response because there is even narrower range of materials able to provide a $\Delta n < 0$.[7] Therefore, the field of optical control requires the development of more efficient nonlinear materials where Δn is controlled under moderate intensities and short distances, and more ambitiously, with a crossover where the (de)focusing response changes with a control parameter varied around a critical/transition point.

In this scenario, it is also of crucial importance the development of the desired optical functionalities within sustainable green technologies, i.e., nontoxic materials and fabrication processes. This would lead to a new generation of ecofriendly devices able to accomplish the new rules imposed by the ecological transition. Here, the extraordinary success of lead halide perovskites (LHPs) in the implementation of highly efficient solar cells or optical sources has derived in the research for equally effective lead-free metal halide perovskite (LFP) semiconductors.[8–11] Many research groups have dedicated

I. Suárez
Escuela Técnica Superior de Ingeniería
Universidad de Valencia
C/Avenida de la Universidad s/n Burjassot, Valencia E-46100, Spain
E-mail: isaac.suarez@uv.es

J. P. Martínez-Pastor, A. Ferrando
UMDO
Instituto de Ciencia de los Materiales
Universidad de Valencia
C/ Catedrático J. Beltrán, 2, Paterna 46980, Spain
E-mail: albert.ferrando@uv.es

M. F. Oszajca, N. A. Lüchinger, B. Graves
Avantama AG
Laubisrütistrasse 50, Stafa 8712, Switzerland

S. Agouram
Dept. Applied Physics & Electromagnetism
Universidad de Valencia
C Dr Moliner 50, Valencia E-46100, Spain

C. Milián
Institut Universitari de Matemàtica Pura i Aplicada
Universitat Politècnica de València
València 46022, Spain

The ORCID identification number(s) for the author(s) of this article can be found under https://doi.org/10.1002/adom.202202120.

DOI: 10.1002/adom.202202120

significant efforts to the synthesis and characterization of effective LFPs, both in bulk and nanocrystal forms.[12] For example, the replacement of Pb^{2+} with divalent Sn^{2+} in the $APbX_3$ compound (A is an organic/inorganic cation and X is an halide anion) leads to the formation of polycrystalline films with moderate photoconversion efficiencies,[13,14] optical gain thresholds close to their LHP counterparts,[15–17] and bandgap tunability with the halide composition.[18] However, $ASnX_3$ perovskites are very sensitive to the ambient atmosphere (oxygen, moisture, and light), where Sn^{2+} is easily oxidized into Sn^{4+} losing its optoelectronic properties. On the other hand, Sn^{4+}-based perovskites, namely, Cs_2SnX_6, which is known as a vacancy ordered double perovskite, exhibit good stability but negligible emission efficiency, even in the case of passivated nanocrystals.[19–21] Then, the optoelectronic applications of Cs_2SnX_6 compounds are reduced to absorbers for solar cells in the case of polycrystalline thin films, and practically discarded in the case of the nanocrystals. Nevertheless, the field of nonlinear optics might provide a panoply of alternative routes that has not yet been explored with Cs_2SnX_6 or other LFPs. In this context, their counterpart LHPs demonstrated excellent perspectives,[7,22] with remarkably high nonlinear coefficients,[23] and promising harmonic generation[24] or optical modulation applications.[25] However, the study of the nonlinear response of an LFP material is reduced to a few publications, as the one focused in the characterization of the two photon absorption mechanism.[26] Therefore, it is mandatary to determine if LFPs present a remarkable nonlinear optical response, as the basis for future nontoxic nonlinear photonic platforms unknown to date.

In this work, we demonstrate that a colloid containing Cs_2SnI_6 nanocrystals (NCs) is an extraordinary self-defocusing material with a nonlinear behavior that has not been observed up to now. These NCs were synthetized by a mechanochemical approach via ball-milling using stoichiometric precursors. This technique allows us to solve the problem of poor solubility of chemical components and provides the formation of LHP compounds in a simple and time-efficient manner.[27–30] The response under an excitation beam at 1064 nm at 1 ns traversing a suspension of these NCs revealed a multiple ring diffraction pattern whose shape and size are controlled by the intensity of the incident beam (I) and the concentration (C) of NCs in the solvent. This behavior indicates that the material under study presents a sophisticated nonlinearity that not only depends on the response of the individual NCs, but also on the collective in a sort of self-assembled superlattice. At these conditions, the determination of an expression for the nonlinear refractive index is a necessary step to design the disruptive functionalities or photonic devices that can be implemented with these NCs. For instance, self-phase modulation (SPM) mechanism induced by a simple Kerr coefficient, i.e., $\Delta n = -n_2 \cdot I$, successfully explains the ring patterns measured in 2D nanosheets in suspensions,[31,32] such as 2D chalcogenides,[33–37] graphene nanosheets,[38,39] black phosphorous,[40,41] carbon nanotubes,[42] antimonene,[43] nonlinear polymers,[44] Bi_2Te_3,[45] $CsPbX_3$ nanosheets,[46] MXene,[47] or TaS_2.[48] However, the I–C dependence observed here implies a more complicated expression for Δn than the standard Kerr effect used for traditional materials. Nevertheless, despite the complexity of the observed experimental results in our compound, our experimental data are fully reproduced with a nonlinear beam propagation method (BPM) that includes a nonlinear refractive index given by: i) a threshold intensity necessary to observe the nonlinear self-defocusing effect, ii) two terms that contain the response of individual NCs and the collective, iii) a negative saturable Kerr nonlinearity ($\Delta n = -\Delta n_o \cdot I/(I+I_d)$) characteristic of the high-order Kerr effect observed in some self-focusing materials,[49] iv) a crossover between two excitation regimes, v) an additional dependence of the nonlinear parameters included in Δn with the C. Importantly, we found $|\Delta n| \sim 10^{-2}$ for the highest excitation intensity (I = 100 MW cm^{-2}), which is two orders of magnitude larger than that reported for 2D materials, silicon, colloidal quantum dots, or LHPs excited under similar conditions.[7] More interestingly, the dependence of the shape of the beam with I and C indicates that Δn follows a phase diagram with four different regions, each with their own superlattice-like behavior. In this way, Δn is engineered from −0.05 to +0.002 with I, C, and the propagation distance (z), which represents a fascinating way to engineer the nonlinear response from self-defocusing to self-focusing. Therefore, the material under study has unique features as a self-defocusing media and will open new routes in the nonlinear field that have not been possible up to now.

2. The Outstanding Self-Defocusing Response of Cs_2SnI_6 Perovskite NCs

The Cs_2SnI_6 NCs under study were synthetized by the ball milling procedure described elsewhere[30] with slight modifications (see the Experimental Section). The transmission electron microscopy (TEM) characterization (**Figure 1**a) indicates that the NCs have ellipsoidal shape and a size distribution centered at 12 nm (Figure 1b). The NCs present cubic structure, as deduced from the high-resolution TEM (HRTEM) analysis, see Section S1 of the Supporting Information (Figure S1, Supporting Information). In agreement with Cs_2SnI_6 NCs prepared by the hot injection method,[50] bigger nanoparticles of 50 ± 10 nm with near hexagonal shape are also visible in some TEM images (Figure S2, Supporting Information) with, again, cubic structure (Figure S3, Supporting Information). The concentration in volume of these hexagonal nanoparticles is, however, a 10–20% of the spherical NCs of 12 nm, approximately, hence its effective influence in the nonlinear optical properties reported in this work is discarded, a priori. According to the analysis developed elsewhere,[51] the quantum confinement effect is very weak for the size of synthesized colloidal NCs (12 nm). Thus, we believe that the size will not give any significant influence to their nonlinear properties. On the other hand, the absorption profile of the NCs in colloidal solution (Figure 1c) indicates the presence of a certain quantum size confinement effect, which causes a well-defined exciton resonance at around 650 nm. This peak is near 20–40 nm blue-shifted with respect to bulk polycrystalline films of the same material,[52,53] which is attributed to a weak confinement effect or some difference in the stoichiometry of the final compound.[52,53] At the wavelength where the nonlinear optical properties are studied (1064 nm), the absorption is negligible.

To characterize the nonlinear properties of the Cs_2SnI_6 NCs, a 1064 nm beam nm is focused on a 1 mm length cuvette filled

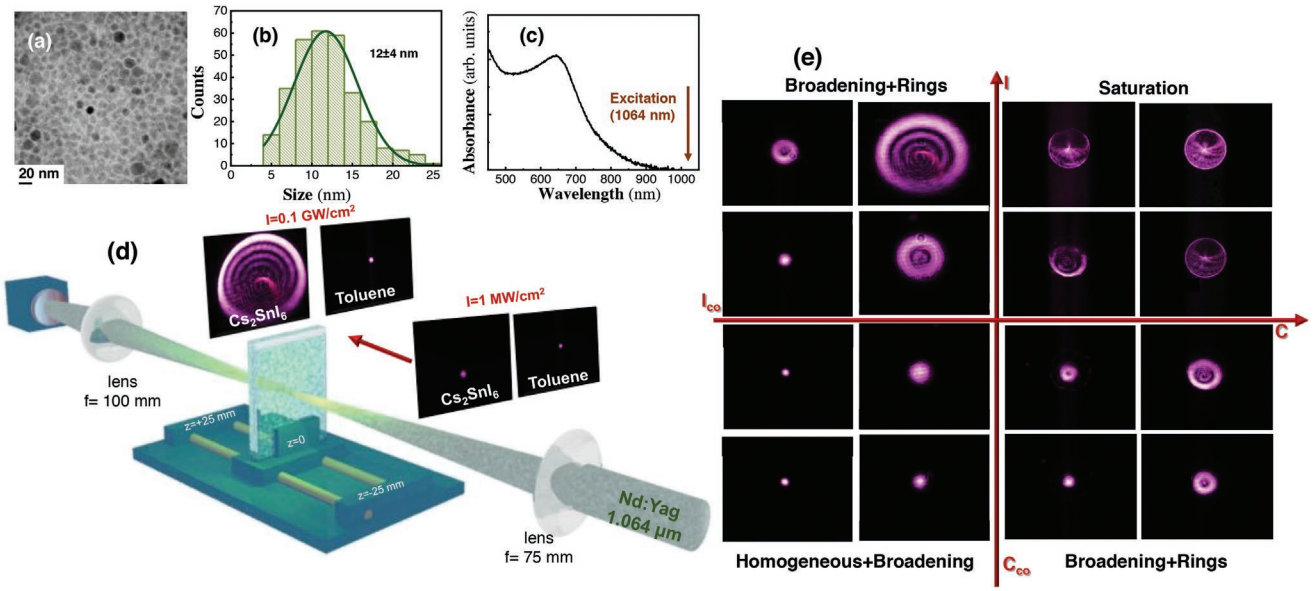

Figure 1. a) TEM images of Cs_2SnI_6 NCs. Scale bar is 20 nm. b) NC size dispersion. c) Absorption spectra of the colloidal solution. d) Experimental set-up used to analyze the nonlinear properties of Cs_2SnI_6 in the colloidal solution. e) Map of the beam patterns as a function of the concentration and excitation intensity.

by the colloidal solution. The laser beam traversing the cuvette was collected with a second lens on a CCD camera to analyze its shape and intensity as function of I, as summarized in the Experimental Section and illustrated in Figure 1d. In all cases, the collection plane is fixed at the output face of the cuvette resulting in very clean near field patterns, as shown in the panels of Figure 1d,e. The inset in Figure 1d shows the images of the beam traversing the cuvette for the toluene and the toluene solution of Cs_2SnI_6 NCs concentrated at 50 mg mL^{-1} for $I = 1$ MW cm^{-2} and $I = 0.1$ GW cm^{-2}. The laser beam traversing the cuvette filled with only toluene (reference) presents negligible changes with I; so, any nonlinear optical effect related with the solvent can be discarded. Nevertheless, when the cuvette is filled with the colloid of Cs_2SnI_6 NCs, the traversing beam experiences a progressive broadening together with a growing number of concentric rings with I. At these conditions, the refractive index of the colloid, n, follows the intensity-dependent law: $n = n_0 + \Delta n(I)$, where n_0 is the linear refractive index of the colloid and $\Delta n(I)$ represents the nonlinear refractive index change. In the case of a standard centrosymmetric crystal, $\Delta n(I)$ is given by

$$\Delta n(I) = n_2 \cdot I - i \cdot \frac{\lambda}{4 \cdot \pi} \cdot \beta \cdot I \quad (1)$$

where λ is the excitation wavelength and the parameters n_2 and β are the nonlinear Kerr and absorption coefficients, respectively. Equation (1) gives a good approximation for moderate values of Δn, where saturation or high-order Kerr effects can be ignored. For example, the ring patterns observed in 2D materials or nanosheets[33–48] were successfully explained by an SPM mechanism derived from the standard Kerr coefficient, n_2. In particular, those publications justify the diffraction ring patterns by an induced birefringence caused by the orientation of the micro/nanoflakes with the incident beam.[54] However, the results presented here show important differences that prevent the use of Equation (1) to estimate n_2. First, the colloidal solution used here consists of ≈12 nm NCs, where the alignment with the incident beam is not expected to produce a significant birefringence. Indeed, the characterization under linear horizontal, linear vertical, and circular polarization gives rise to the same ring patterns (see Figure S4, Supporting Information). Second, in those publications the excitation wavelength is always chosen below the bandgap of the semiconductor. Otherwise, the electromagnetic interaction results too low to induce an appreciable Kerr effect and the ring patterns are not observed.[39] On the contrary, in the experiment carried out here, the nanocrystals are excited in the IR (1064 nm), which is a photon energy well below the absorption band edge of the material (see Figure 1c). More importantly, in those publications the absolute value of the nonlinear refractive index ($|n_2|$) is extracted by the number of the rings (N) with the formula (see Section S2 of the Supporting Information):[32,55] $N(I) = \frac{2 \cdot n_0 \cdot L_{\text{eff}}}{\lambda} |n_2| \cdot I$, where L_{eff} is the effective propagation length. However, the $N(I)$ dependence is only valid for small $|\Delta n|$, where the self-diffraction caused by the Kerr effect is negligible and the electric field patterns can be approximated by the Fresnel–Kirchhoff diffraction theory (see Section S4, Supporting Information).[56–59] In these previous publications, where $|\Delta n| \sim 10^{-4}$, this approximation was acceptable, but the high Δn found here prevents its use to extract the right value of n_2. In fact, for the ring pattern shown in Figure 1d $|n_2| = 0.027$ GW cm^{-2} and the resulting refractive index change ($\Delta n = n_2 \cdot I$) from Equation (1) reaches $|\Delta n| \sim 10^{-3}$ (for 100 MW cm^{-2}). Furthermore, since N is always a positive number, the dependence of n_2 with N can yield the absolute value of n_2, but it does not discriminate the sign. Finally, the colloidal solution studied

here shows a particular dependence with I and C that cannot be explained globally by the single n_2 coefficient given by Equation (1). The panels of Figure 1e reveal that the evolution of the beam as a function of I and C shows different regions delimited by a crossover in the concentration (C_{co}) and the intensity (I_{co}): i) for $C < C_{co}$ and $I < I_{co}$, the beam exhibits a homogenous Gaussian shape with a progressive broadening with C and I; ii) for $C < C_{co}$ and $I > I_{co}$, the beam traversing the cuvette shows a growing number of concentric rings with I; iii) for $C > C_{co}$ and $I < I_{co}$, the beam experiences a fast broadening together with the appearance of the rings; iv) for $C > C_{co}$ and $I > I_{co}$, the shape and size of the ring pattern saturate. Since each region presents a particular behavior, we believe that above a certain threshold of excitation intensity (I_{th}) the nonlinear behavior of the colloid is enhanced by a collective effect. In this way, C_{co} is attributed to border concentration from which the nonlinear behavior is dominated by the ensemble and I_{co} refers to the saturation intensity for the collective response. At these conditions, these four regions are characterized by a certain distribution of NCs around the excitation beam, and a nontrivial dependence of Δn with I, C, the radial distance (r), and the propagation distance (z). This complex behavior is understood here by using the nonlinear Schrödinger equation to calculate the propagation of the excitation beam through the nonlinear media.[60] For this purpose, the nonlinear BPM algorithm described in Section S5 of the Supporting Information (see the illustration in Figure S5, Supporting Information) accurately simulates the evolution of an incident electric field through an arbitrary refractive index distribution.[61] In particular, the BPM algorithm is able to reproduce the experimental patterns (see Figure S6, Supporting Information) by considering the following type of nonlinearity dependent on the excitation intensity, $I(r,z)$, and concentration, C

$$\Delta n\left(I(r,z),C,r,z\right)=\alpha_{NC}(I)\,\mathcal{N}(I,C)-i\cdot\frac{\lambda}{4\cdot\pi}\cdot\beta\cdot I(r,z)$$
$$\alpha_{NC}(I)=-\Delta n_0\cdot\frac{I(r,z)}{I(r,z)+I_d(C)} \quad (2)$$
$$\mathcal{N}(I,C)=k(C)\cdot\frac{I(r,z)-I_{th}(C)}{I(r,z)+I_{co}(C)}\cdot\exp\left(-\frac{r^2}{w_r^2}\right)$$

where the different parameters are defined as follows:

i) Δn_0: saturable nonlinear refractive index of the individual nanoparticles;
ii) β: nonlinear absorption parameter;
iii) λ: operation wavelength;
iv) $I_d(C)$: saturation intensity of the individual nanoparticles;
v) $k(C)$: enhancement of the nonlinear refractive index due to the collective response;
vi) $I_{th}(C)$: minimum intensity to observe the nonlinear response;
vii) $I_{co}(C)$: collective saturation intensity;
viii) w_r: width of the self-formed waveguide, fixed as 20 µm (half the waist of the beam);
ix) r: radial distance;
x) z: propagation distance.

The two terms from which Equation (2) is divided, $\alpha_{NC}(I)$ and $\mathcal{N}(I,C)$, correspond to the response of the individual NCs and that of the collective, respectively. Both terms have the form of a saturable Kerr nonlinearity,[62] which was previously proposed to explain the nonlinear behavior of photorefractive crystals.[63] Equation (2) is completed by a threshold (I_{th}) below which the nonlinear effects are negligible and an exponential term referring to the self-formation of an induced (anti)waveguide with a width of $w_r = 20$ mm. Finally, the negative sign indicates that the material diluted at this concentration is a potential self-defocusing media. Indeed, the simulation with a standard Δn given by Equation (2) suggests the necessity of negative values for n_2 to qualitatively reproduce the experimentally observed field patterns (see Figure S7, Supporting Information). For a further confirmation of the sign of n_2, we repeated the experiment by placing the cuvette with the colloid of LFP NCs at $z = \pm 25$ mm (Figure 1d). At these positions, the cuvette is outside the Rayleigh range, hence it is illuminated with a finite curvature radius (R) whose sign is opposite at $z = +25$ mm and $z = -25$ mm: if $R\Delta n < 0$, the far field pattern is composed by a central dark spot surrounded by thick concentric ring, while if $R\Delta n > 0$, the pattern will consist of a central bright spot with thin concentric rings,[57–59] as observed experimentally (Figure S8a,b, Supporting Information). In the following, we explain the nature of all parameters involved in Equation (2) and what is the particular response at each region of the map shown in Figure 1e.

3. Determination of the Giant Self-Defocusing Nonlinearity

When the cuvette is filled with $C = 50$ mg mL^{-1} (initial concentration), the shape and size of the traversing beam show the evolution with I illustrated in **Figure 2**a. There are two regions with different behavior for the transmitted laser beam. For low excitation intensities, below the crossover ($I < I_{co} \approx 0.01$ GW cm^{-2}), the traversing beam shows a progressive broadening with the excitation intensity (images in this regime are grouped by a dark yellow rectangle in the four top-left panels of Figure 2a). However, for $I > I_{co}$ the near-field pattern presents a dark central spot surrounded by the appearance of a growing number of concentric rings (images grouped by a red rectangle) in the five top-right panels of Figure 2a. The ring asymmetry of the laser beam images after traversing the colloid with NCs is produced by a slight ellipticity (less than 10%) of the incident beam.

The optical nonlinearities observed in the Cs_2SnI_6 colloid can be determined by the analysis of the images presented in Figure 2a, as follows. First, the transmittance (T) is obtained by the ratio between the intensity of the beam traversing the colloidal solution and that of the beam traversing the toluene. The experimental dependence of T as a function of I (solid symbols in Figure 2b) exhibits a progressive decrease characteristic of a nonnegligible nonlinear absorption ($\beta > 0$).[23] In fact, the experimental data can be nicely fitted (solid line in Figure 2b) by the characteristic equation for two photon absorption, $dI/dz = -\beta\cdot I^2$,[64] with $\beta = 80$–100 cm GW^{-1}. On the other hand, the evolution of the laser beam shape by increasing I reflects the magnitude of the real part of the nonlinear refractive index. Left axis of Figure 2c presents the beam waist (w) of the colloidal dispersions of LFP NCs normalized to its value measured under low excitation conditions (w_0) as a function of I (right axis of the figure was scaled

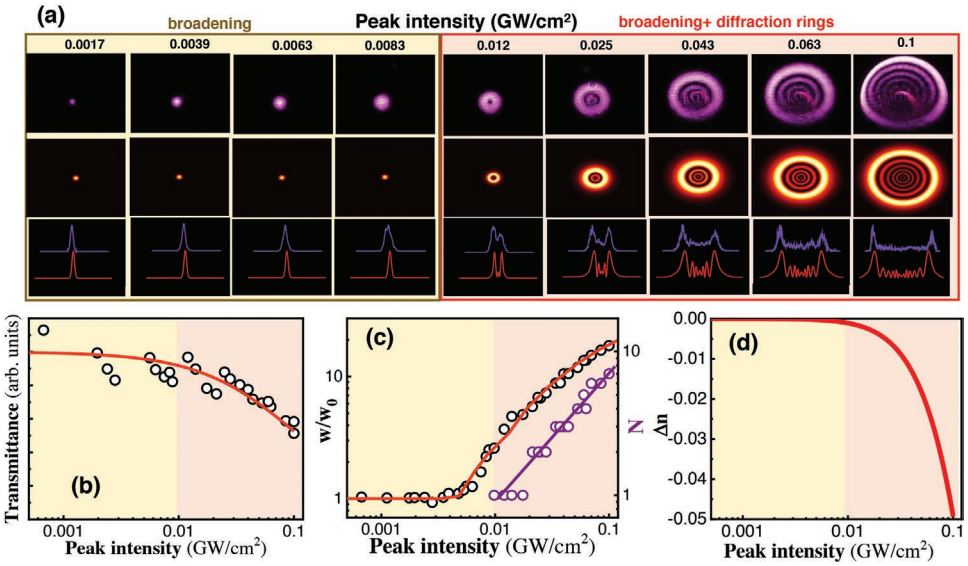

Figure 2. a) Characterization and simulation of the near field at the exit of the cuvette for different peak excitation intensities. Top panels show the experimental (purple) and simulated (red) maps, and bottom panels the horizontal cross-section of the experiment (purple) and simulation (red). b) Transmittance as a function of the peak intensity indicates a nonlinear absorption $\beta = 80$–100 cm^2 GW^{-1}. c) Left axis. Log–log plot of the experimental size of the beam (black open symbols) and fitting (red solid line) with a saturable Kerr-type nonlinearity. Right axis. Log–log plot of the number of rings (purple open symbols). d) Refractive index change at each excitation region.

to give the number of rings, N, as a function of I). The evolution of $w(I)/w_0$ is characterized by the following features: i) there is a threshold (I_{th}) above which the nonlinear effect is observed; ii) for $I_{th} < I < I_{co}$, the beam experiences a slow broadening that can be associated with the images by a dark yellow rectangle in Figure 2a; for $I > I_{co}$, the beam experiences a fast broadening that can be related with the appearance of the concentric rings (red rectangle in Figure 2a), where the outermost ring diameter (w) reaches up to 20 times the initial beam size (w_0). Despite the complexity of the material and the experimental results, the nonlinear BPM algorithm correctly identifies the nature of the optical nonlinearity (negative/positive n_2) and extracts the right parameters involving Δn and β for the case under study (Cs_2SnI_6 NCs here). Indeed, the particular nonlinearity given by Equation (2) well reproduces the behavior of our experimental data by setting $I_d >> I$ (see approximation in Supporting Information Section S9), $I_{th} = 1.4 \times 10^{-3}$ GW cm^{-2}, $I_{co} = 0.02$–0.05 GW cm^{-2}, and $k \cdot \Delta n_o / I_d = 0.6$–$0.75$ cm^2 GW^{-1}.

As a matter of fact, our simulations not only reproduce qualitatively the field patterns shown in Figure 2a (spectacular in the case of the high fluence regime), but also quantitatively the shape of the transmitted beam, see the simulation of the Poynting vector in the middle panels and comparison of the cross-sections (simulation and experiment) at the bottom panels. The small disagreement in the left part of the panels is attributed to the fact that the beam is not purely Gaussian but contains a tail that is visible in the images with an apparent more important broadening. Nevertheless, the comparison of the intensity profiles, see bottom panels in Figure 2a, corroborates that there is quite good agreement between experiment and simulations. In fact, the log–log plot of the normalized beam waist as a function of the excitation intensity, open symbols in Figure 2c, clearly shows a good correspondence between experiment and simulation. Figure 2d plots the Δn obtained for $z = 0$ as a function of the peak intensity: Δn is always negative and above $I_{co} = 0.01$ GW cm^{-2} (red shaded region), it exhibits a remarkable increase in absolute value, up to $|\Delta n| \approx 0.05$, corroborating that the suspension of LFP NCs under consideration is an outstanding self-defocusing medium for nonlinear optics. Indeed, the results obtained here represent record values for the negative Δn obtained with perovskite-like nanomaterials.[7] Table S2 in the Supporting Information presents the nonlinear coefficients obtained from the Z-scan characterization of LHP thin films ($MAPbX_3$, MA = methylammonium X = Br,I) and nanocrystals ($CsPbX_3$, X = Br, I) using the same experimental setup and excitation conditions (1 ns pulsed laser at 1064 nm). In this way, we can say that the absolute value of our Δn is two to three orders of magnitude higher than that previously measured for LHPs NCs, and similar in absolute value of polycrystalline thin films of LHPs.[23] The stronger nonlinear response of the NCs under study could be initially related with their vacancy ordered double lattice (A_2BX_6), which differs from that of LHP materials (ABX_3). At the same time, this value is also much higher than those reported for Si, InP,[65] and transition metal dichalcogenides in solid-state phase, see Table S2, Supporting Information.[66] More interestingly, the highest peak intensity used here corresponds to an average power of <100 mW, which is below the excitations reported for self-defocusing applications.[4–6] Therefore, we believe that the NCs used in the present work will allow new regimes and applications in nonlinear photonics that have not been considered up to now.

4. Dependence of the Nonlinear Response with the Concentration

To deeply validate the influence of the collective term, $\mathcal{N}(I,C)$, introduced in Equation (2) the experiment was carried out

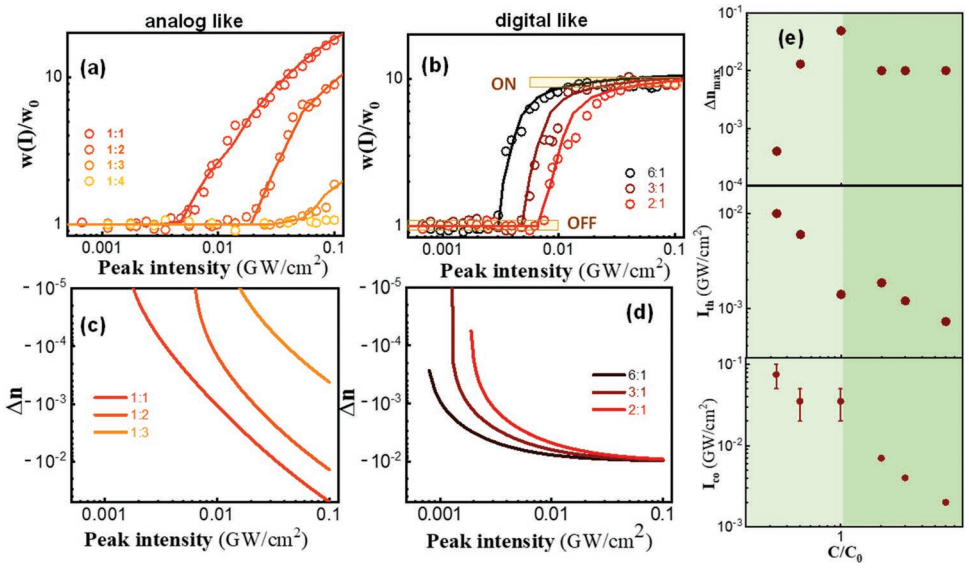

Figure 3. Log–log plot of the beam width as function of the peak intensity: a) low concentration (1:1, 1:2, 1:3, 1:4), b) high concentration (6:1, 3:1, 2:1). Symbols correspond to the experimental data and solid lines to the modeling. Δn as function of the peak intensity: c) low concentration (1:1, 1:2, 1:3, 1:4), d) high concentration (6:1, 3:1, 2:1). e) Parameters extracted from the modeling (Δn at 0.1 GW cm^{-2}, I_{th}, I_{co}) as a function of the concentration.

under different concentrations of the NCs in the solvent. First, the experiment realized with diluted solutions indicates a smaller effective Δn. A solution diluted at 50% shows a reduced broadening above a threshold of around 0.005 GW cm^{-2} and the appearance of rings above a crossover $I_{co} \approx 0.03$ GW cm^{-2} (orange symbols in **Figure 3**a and Figure S9, Supporting Information), the dilution at 33.3% only shows the broadening region for $I_{th} > 0.01$ GW cm^{-2} (light orange symbols in Figure 3a) and a dilution at 5–25% does not exhibit any nonlinear effect at all (yellow symbols in Figure 3a) within the available laser excitation intensities. In all cases, we can say that the shape of the beam shows a rather smooth dependence with I whose slope and threshold are tuned by C. At these conditions, the colloid presents an analogl-like performance useful for applications where a continuous variation with the intensity is required (i.e., analogical modulation, sensing,...). On the opposite, when the solution is concentrated above the initial concentration (6:1, 3:1, and 2:1), the evolution of the beam with I presents the rather abrupt behavior shown in Figure 3b. The broadening observed above the threshold (I_{th}) has a much faster growth and is always accompanied with the appearance of growing rings. Besides, there is also an I_{co} above which the beam waist saturates reaching a plateau where the number of rings is constant: $I_{co} \approx 0.003$–0.005, $I_{co} \approx 0.005$–0.008, and $I_{co} \approx 0.008$–0.01 GW cm^{-2} for C = 600%, C = 300%, and C = 200%, respectively. In this way, the colloid behaves as a digital-like system switched from an OFF (or weak nonlinear material) to an ON (strong nonlinear material) state above a C-dependent threshold. Potential applications include digital modulation, computing, or data processing. Therefore, the observed dependence of $w(I)$ with C represents a straightforward method to choose the nonlinear functionalities and indicates that the potential applications of the colloid can be tailor-made.

In both cases, low and high C behaviors, we believe that the concentration of NCs in the solvent modifies the effective refractive index of the solution, as occurs in a solid nanocomposite filled by nanoparticles.[67] In this way, experimental w–I curve obtained with the solutions diluted is fitted with Equation (2) with the appropriate parameters, see solid lines in Figure 3a,b. For low C, the conditions $I_d >> I$, I_{co} = 0.02–0.05 GW cm^{-2}, and w_r = 20 µm are also necessary to reproduce the beam traversing the diluted solutions (C = 33% and C = 50%), but the simulation indicates a smaller $k \cdot \Delta n_o / I_d$ (see Tables S3 and S4, Supporting Information), which leads to the expected reduction of Δn (see Figure 3c). For high C, the BPM can reproduce the experimental data (solid lines in Figure 3c) by setting $I << I_d$ which leads to a standard saturable Kerr nonlinearity[62] modulated by an exponential term (see Supporting Information Section S9). In particular, the three concentrations are fitted with the same $k \cdot \Delta n_o = 0.01$ and $w_r = 20$ µm, but with a decreasing I_{th} and I_{co} with C (see Tables S3 and S4, Supporting Information). As expected, Δn increases with C and I and saturates for the highest excitations.

Both limits of Equation (2), high and low C, are indicative that high-order Kerr nonlinearities can play an important role.[63] Equation (2) can be expanded in the Taylor series $\Delta n = n_2 \cdot I + n_4 \cdot I^2 + n_6 \cdot I^3 + \cdots$, with the nonlinear coefficients n_2, n_4, n_6 ... for the low and high C limits described in the Supporting Information Section S9. A similar effect has been observed in light-pulse filamentation, where an air plasma evolves from self-focusing to self-defocusing under ultrashort pulses (fs) and extreme light intensities (TW cm^{-2}).[68] Nevertheless, this effect is observed here for a self-defocusing media and relatively low excitation intensities and much longer (ns) pulses. Moreover, the different form of the coefficients obtained by this expansion reveals that each regime is dominated by a different nonlinearity and corroborates that there is a crossover concentration (C_{co}) between both regimes. Figure 3e plots the parameters I_{co} and I_{th} extracted from the model and the maximum Δn as a function of C. As commented, both I_{co}

and I_{th} decreases with C, and also the difference $I_{co} - I_{th}$ which becomes ≈0 for $I > I_{co}$. Interestingly, the extracted values of I_{co} for all concentrations are close to the experimental intensities from which the concentric rings are observed, hence this parameter can be associated with the formation of the rings. Finally, the maximum Δn grows with C up to $\Delta n \approx -5 \times 10^{-2}$ for $C = 100\%$ and saturates up to $\Delta n = 10^{-2}$ for $C = 200$–600%. Here, the region between $C = 100\%$ and $C = 200\%$ can be understood as an intermediate region influenced by both the individual and collective response in Equation (2).

4.1. Concentration–Intensity phase diagram

At this point, it is interesting to analyze the evolution of Δn with the propagation distance (z) for the four regimes/phases that were identified above (Figure 1e):

IIA) $C < C_{co}$ and $I < I_{co}$
IIB) $C > C_{co}$ and $I < I_{co}$
III) $C > C_{co}$ and $I < I_{co}$
IV) $C > C_{co}$ and $I > I_{co}$.

Figure 4a shows the calculation of the $\Delta n(r = 0,z)$ for these four phases and the inset represents the 3D plot of $\Delta n(r,z)$ for a fixed I and C. For $C < C_{co}$, the negative Δn is low and decreases in absolute value with z until a constant refractive index $\Delta n \to 0$. When $I < I_{co}$ (region IIA), the beam is defocused with $\Delta n \approx -10^{-3}$ only in the first microns of the propagation ($z < 10$ µm), causing the observed slight beam broadening in the focal region.[69] For $I > I_{co}$ (region III), the nonlinear response reaches a stronger negative value of around $\Delta n \approx -10^{-2}$ and decreases slowly until $z > 200$ µm, where the nonlinear effect tends to disappear due to low values of $I(r, z)$ produced by strong beam broadening (so that, $\Delta n \to 0$). From this distance onward the beam propagates linearly (see the corresponding inset), but the accumulated Δn results on the necessary nontrivial phase distribution to generate the observed ring patterns, in analogy with an SPM measured with 2D nanosheets.[33–48] A similar behavior is observed for $C > C_{co}$ and $I < I_{co}$ (region IIB), but with a sharper dependence on z. Consequently, the beam experiences generation of rings with I together with broadening. Finally, for $C > C_{co}$ and $I > I_{co}$ (region IV), Δn presents a much progressive evolution with z from $\Delta n \approx -10^{-2}$ to $\Delta n \approx 2 \times 10^{-3}$. Here, clearly we observe a change from self-defocusing to self-focusing at long propagation distances ($z > 0.7$ mm) resulting in a *self-induced waveguide* that maintains the shape of the beam (see the corresponding inset). To the best of our knowledge, this is the first time where a transition from positive to negative Δn is demonstrated with the propagation distance. The cause of this transition is the saturation of the negative nonlinear response imposed by the collective term $N(I,C)$ in Equation (2) when $I >> I_{co}$, I_{th}, and C/C_{co}. At these conditions, the shape of the beam remains constant with I (see Figure 3c) as it propagates through the *self-induced waveguide*. A similar effect was postulated in the context of filamentation in plasmas, but this behavior is observed under much higher excitation intensities.[70] Indeed, the inclusion of high-order Kerr terms has already been chosen to explain the saturation of the nonlinear refractive index observed in photorefractive materials,[62] gases,[49] or the aforementioned light-pulse filamentation.[71] Contrary to these publications, here we can tune the sign of Δn and obtain higher absolute values under smaller propagation distances and excitation intensities.

Finally, it is interesting to postulate the origin of the observed behavior, especially the observed low-to-high excitation evolution, the dependence on the concentration and the transition from self-defocusing to self-focusing. On the one hand, the optical Kerr effect has been chosen to explain the diffraction rings observed for micro and nanoflakes.[33–38,40,42–45] Besides, it has been also demonstrated that the sign of birefringence (Δn) can be positive or negative depending on if the electric field is parallel or perpendicular to the induced dipoles, respectively.[72] However, this effect was discarded because of the small size of the NCs used here (10 nm NCs) and the absence of the dependence with the polarization (see Figure S4, Supporting Information). Thus, we believe that the origin of the observed nonlinear effect comes from an effective modification of the refractive index due to a collective effect in the aggregation of NCs in the excitation volume. The cause of this aggregation can be attributed to the electromagnetic force developed here under sufficiently high intensities.

The map of Figure 4b reinterprets Figure 1a with the dependence of $\Delta n(0,0)$ as a function of I and C. The black lines on

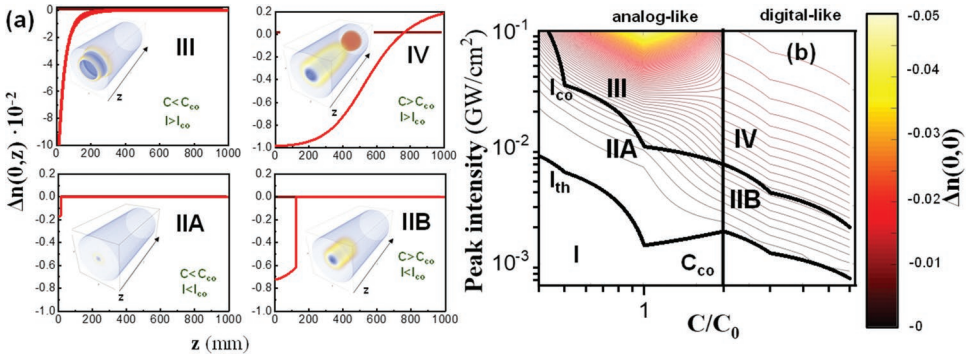

Figure 4. Simulation of $\Delta n(r,z)$ with Equation (2). a) The four different regimes shown in Figure 1e present a different evolution of $\Delta n(0,z)$ at the four different regions: IIA) Broadening, IIB) Fast Broadening+Rings, III) Slow Broadening+Rings, and IV) Saturation. Brown line indicates $\Delta n = 0$. Inset shows a 3D plot of $n(r,z)$. b) $\Delta n(0,0)$ map plotted versus the peak intensity and the concentration show the four different phases.

the map indicate the parameters I_{th}, I_{co}, and C_{co} extracted from the modeling. When $I < I_{th}$, the nonlinear effect is negligible, and the solution takes place in a homogenous phase with $\Delta n \approx 0$ (region I in the figure). This threshold represents the minimum excitation to modify the refractive index in the solvent and plays an analogous role as the Freedericksz transition found in liquid crystals.[32] For $I > I_{th}$, the beam experiences a broadening due to a negative Δn where the four regions described in Figure 4a are delimited by the I_{co} and C_{co} curves. Such a particular dependence of Δn with C and I suggests a collective mechanism in which the beam intensity also modifies the concentration of NCs in the solvent in a sort of light-induced superlattice/aggregate. We would be more inclined to think of a certain disordered/ordered phase transition, because it continuous to be observed by increasing the NC concentration, as observed in Figure 3a,b.

Assuming a dilute particle approximation for the NC solution and identical dipole response for every NC, the macroscopic polarizability in a macroscopic volume of NCs can be approximated by $P = \mathcal{N}p$, where $\mathcal{N}$ is the nanoparticle density and p is the individual induced dipole moment in the NC. In this approximation, the variation of the refractive index due to NCs with respect to that of the solvent is also proportional to $\mathcal{N}$: $\Delta n = \mathcal{N}\alpha_{NC}$, where α_{NC} is the polarizability of a single NC. Clearly, α_{NC} has a nonlinear response with the field intensity due to the intrinsic nonlinearities of the material forming the NC. However, if this was the only origin of optical nonlinearities in the colloid, the ratio between the index variation Δn at two different concentrations of NCs should be independent of the beam intensity $\Delta n_2(I)/\Delta n_1(I) = \mathcal{N}_2/\mathcal{N}_1$. Experimental results of the refractive index change in Figure 4b for different concentrations (i.e., different $\mathcal{N}$s)contradict this behavior since they show that this ratio, indeed, depends on beam intensity. This is an indication that there must be an additional intensity dependence on the NC density $\mathcal{N}(I)$, $\Delta n(I) = \mathcal{N}(I)\alpha_{NC}(I)$ as already postulated in Equation (2) in order to reproduce the experimental results. In fact, an intensity-independent $\mathcal{N}$ would produce identical shapes for $\Delta n(I)$ only distinguished by a scale factor. Contrarily, the shape of the Δn curve not only changes with I but also for different concentrations, see Figure 4b. In our numerical model, this behavior can be attributed to an NC density of the form $\mathcal{N}(I;\mathcal{N}_0)$, where $\mathcal{N}_0$ is the original NC concentration, i.e., $\mathcal{N}_0 = \mathcal{N}(0;\mathcal{N}_0)$. This result points out that the spatial distribution of NC dipoles is qualitatively different depending on the beam peak intensity. High values of $\mathcal{N}$ indicating a large localization of NCs are achieved at high intensities, whereas unmodified values of $\mathcal{N}$ occur at weak intensities.[73] These two collective regimes for $\mathcal{N}$ at high and low peak intensities are connected by the threshold and crossover intensities (I_{th} and I_{co}) that dictates the boundaries between the different regimes (I–C phases). It is worth mentioning that for $C < C_{co}$ and $I < I_{co}$ the system approximates to the individual NC response. On the opposite, the results obtained for $C > C_{co}$ and $I < I_{co}$ indicate that the nonlinear response saturates as we observe experimentally. The microscopic collective mechanism that can explain this behavior of the NC density is still under consideration. Trapping of NCs by the optical beam, as in optical tweezers, can be the driving force for such disorder/order phase transition, as a potential explanation. In this situation, nanoparticles with refractive index higher than that of the surrounding medium are attracted toward the high-intensity region of the optical field, thus generating an increase of the particle density $\mathcal{N}$ where I is higher.[74]

5. Conclusions

In this manuscript, we demonstrate that the nontoxic Cs_2SnI_6 LFPs NCs in solution is an extraordinary defocusing media with outstanding nonlinear properties not yet observed with any other material. The transmittance of a focused beam traversing the cuvette filled by the solution of NCs revealed a set of concentric rings whose number, width, and shape depend on the intensity of the beam and the concentration of NCs in the solvent. This fascinating behavior is completely and non-trivially reproduced with a BPM algorithm incorporating a nonlinearity composed by two negative saturable nonlinear effects corresponding to the response of the individual NCs/nanoparticles and a collective mechanism (such as ordering, e.g.). Both experiment and model indicate a dependence of Δn with I and C with four operation/propagation regimes or phases delimited by intensity and concentration crossovers. In each phase, Δn exhibits a particular dependence with I, which represents a straightforward method to select the nonlinear functionalities. Indeed, moving along the phase diagram at a specific propagation distance, Δn can be tuned from -5×10^{-2} to $+2 \times 10^{-3}$, leading to the formation of the self-induced (anti) waveguides required to develop sophisticated nonlinear applications, such as shocks, polaritons, dark solitons, and others. For certain I and C values, the induced nonlinear index contrast can achieve the extreme value $\Delta n = -5 \times 10^{-2}$, which is the strongest defocusing response reported up to now, to the best of our knowledge. Moreover, this Δn is reached under only moderate average laser average powers <100 mW, intensities as low as 50 MW cm^{-2}, indicating that these colloidal suspensions of LFP NCs can be potential materials for the nonlinear optics field and can pave the road to disruptive photonic applications not achievable up to now.

6. Experimental Section

Materials and Synthesis of the Nanocrystals: Synthesis of Cs_2SnI_6 nanoparticles was made by ball milling, following the procedure described elsewhere[30] with slight modifications. All chemicals were purchased from Sigma Aldrich and used without further purification. In order to obtain the highest monodispersity of the nanoparticles,[21] the bulk Cs_2SnI_6 phase was first obtained by dry milling. 8 mmol of CsI (99.9%) and 4 mmol of SnI_4 (99.999%) was mounted into a zirconia bowl together with ≈20 milling beads of 5 mm in diameter and milled in a planetary ball mill for 3 h at speed of 300 rpm. In this way, 0.5 g of the obtained black powder was mounted in a separate zirconia bowl followed by 15 g of toluene (99.8%), 0.1 g of oleic acid (90%), 0.1 g of oleylamine (98%), and same amount of milling beads. The bowl was sealed with a Viton O-ring and milled for 3 h at 500 rpm. The resulting black dispersion was centrifuged for 10 min at 3750 rpm and the supernatant was used for further tests.

TEM Analysis: Morphological, compositional, and structural analysis of the nanoparticles was performed by HRTEM with a field emission gun TECNAI G2 F20 microscope operated at 200 kV, having the capabilities of selected area electron diffraction and energy dispersive

X-ray spectroscopy in the facilities of the Servei Central de Suport a la Investigació Experimental (SCSIE) at the University of Valencia.

Optical Characterization: Absorption spectra in the colloidal solution were measured with a commercial HP8453 UV-VIS spectrometer equipped with a diode array sensor and deuterium/halogen lamps.

The nonlinear optical properties of the samples were characterized by illuminating the colloidal solutions (40 mg mL^{-1}) dispersed in a 1 mm cuvette with a 1064 nm Nd:Yag laser (1 ns, 20 kHz) Gaussian beam. The beam was focused with a 75 mm focal lens, leading to a waist and Rayleigh distance of w_0 = 35–40 µm and z_R = 3.5–5 mm, respectively. In this way, the cuvette length (1 mm) accomplished the thin sample approximation criteria (z_R > thickness of the sample).[75] The transmitted light was analyzed as a function of the peak excitation intensity in the range 1–100 MW cm^{-2}. A 100 mm focal lens was used to collect the transmitted light by a Thorlabs CCD DCU224M camera.

Supporting Information

Supporting Information is available from the Wiley Online Library or from the author.

Acknowledgements

This project has received funding from the European Union's Horizon 2020 research and innovation programme under grant agreement no. 862656 (project DROP-IT) and by the Spanish MICINN through project no. PID2020-120484RB-I00 and by Generalitat Valenciana PROMETEO/2021/082.

Conflict of Interest

The authors declare no conflict of interest.

Authors Contribution

I.S., J.M.P., and A.F. conceived the study. M.F.O., N.A.L., and B.G.G. synthetized the colloidal nanocrystals. I.S. did the optical characterization, simulations, and modeling. S.A. performed the TEM analysis. I.S., J.M.P., C.M., and A.F. discussed the data. I.S. prepared the original draft of the manuscript. I.S., J.M.P., C.M., and A.F. participated in the writing and reviewing the manuscript.

Data Availability Statement

The data that support the findings of this study are available from the corresponding author upon reasonable request.

Keywords

Cs_2SnI_6, Kerr effect, lead free perovskites, nonlinear, phase transition, self-defocusing

Received: September 9, 2022
Revised: October 15, 2022
Published online: November 21, 2022

[1] R. W. Boyd, *Nonlinear Optics* Elsevier, Rochester, NY **2007**.
[2] M. Taghinejad, W. Cai, *ACS Photonics* **2019**, *6*, 1082.
[3] J. Leuthold, C. Koos, W. Freude, *Nat. Photonics* **2010**, *4*, 535.
[4] M. J. Jacquet, T. Boulier, F. Claude, A. Maître, E. Cancellieri, C. Adrados, A. Amo, S. Pigeon, Q. Glorieux, A. Bramati, E. Giacobino, *Philos. Trans. R. Soc., A* **2020**, *378*, 20190225.
[5] J. Wang, J. Li, D. Lu, Q. Guo, W. Hu, *Phys. Rev. A: At., Mol., Opt. Phys.* **2015**, *91*, 2.
[6] V. Smith, B. Leung, P. Cala, Z. Chen, W. Man, *Opt. Mater. Express* **2014**, *4*, 1807.
[7] A. Ferrando, J. P. Martínez Pastor, I. Suárez, *J. Phys. Chem. Lett.* **2018**, *9*, 5612.
[8] F. Giustino, H. J. Snaith, *ACS Energy Lett.* **2016**, *1*, 1233.
[9] J. Sun, J. Yang, J. I. Lee, J. H. Cho, M. S. Kang, *J. Phys. Chem. Lett.* **2018**, *9*, 1573.
[10] A. Abate, *Joule* **2017**, *1*, 659.
[11] R. Wang, J. Wang, S. Tan, Y. Duan, Z. K. Wang, Y. Yang, *Trends Chem.* **2019**, *1*, 368.
[12] Q. Fan, G. V. Biesold-McGee, J. Ma, Q. Xu, S. Pan, J. Peng, Z. Lin, *Angew. Chem., Int. Ed.* **2020**, *59*, 1030.
[13] K. P. Marshall, M. Walker, R. I. Walton, R. A. Hatton, *Nat. Energy* **2016**, *1*, 16178.
[14] F. Hao, C. C. Stoumpos, D. H. Cao, R. P. H. Chang, M. G. Kanatzidis, *Nat. Photonics* **2014**, *8*, 489.
[15] R. L. Milot, G. E. Eperon, T. Green, H. J. Snaith, M. B. Johnston, L. M. Herz, *J. Phys. Chem. Lett.* **2016**, *7*, 4178.
[16] P. Ščajev, R. N. Aleksiejūnas, P. Baronas, D. Litvinas, M. Kolenda, C. Qin, T. Fujihara, T. Matsushima, C. Adachi, S. Juršėnas, *J. Phys. Chem. C* **2019**, *123*, 19275.
[17] G. Xing, M. H. Kumar, W. K. Chong, X. Liu, Y. Cai, H. Ding, M. Asta, M. Grätzel, S. Mhaisalkar, N. Mathews, T. C. Sum, *Adv. Mater.* **2016**, *28*, 8191.
[18] T. C. Jellicoe, J. M. Richter, H. F. J. Glass, M. Tabachnyk, R. Brady, S. E. Dutton, A. Rao, R. H. Friend, D. Credgington, N. C. Greenham, M. L. Böhm, *J. Am. Chem. Soc.* **2016**, *138*, 2941.
[19] A. Wang, X. Yan, M. Zhang, S. Sun, M. Yang, W. Shen, X. Pan, P. Wang, Z. Deng, *Chem. Mater.* **2016**, *28*, 8132.
[20] D. S. Dolzhnikov, C. Wang, Y. Xu, M. G. Kanatzidis, E. A. Weiss, *Chem. Mater.* **2017**, *29*, 7901.
[21] A. Veronese, M. Patrini, D. Bajoni, C. Ciarrocchi, P. Quadrelli, L. Malavasi, *Front. Chem.* **2020**, *8*, 35.
[22] J. Xu, X. Li, J. Xiong, C. Yuan, S. Semin, T. Rasing, X. Bu, *Adv. Mater.* **2019**, *32*, 1806736.
[23] I. Suárez, M. Vallés-Pelarda, A. F. Gualdrón-Reyes, I. Mora-Seró, A. Ferrando, H. Michinel, J. R. Salgueiro, J. P. M. Pastor, *APL Mater.* **2019**, *7*, 041106.
[24] I. Abdelwahab, G. Grinblat, K. Leng, Y. Li, X. Chi, A. Rusydi, S. A. Maier, K. P. Loh, *ACS Nano* **2018**, *12*, 644.
[25] G. Grinblat, I. Abdelwahab, M. P. Nielsen, P. Dichtl, K. Leng, R. F. Oulton, K. P. Loh, S. A. Maier, *ACS Nano* **2019**, *13*, 9504.
[26] A. Mushtaq, B. Pradhan, D. Kushavah, Y. Zhang, M. Wolf, N. Schrenker, E. Fron, S. Bals, J. Hofkens, E. Debroye, S. K. Pal, *ACS Photonics* **2021**, *8*, 3365.
[27] Y. El Ajjouri, F. Palazon, M. Sessolo, H. J. Bolink, *Chem. Mater.* **2018**, *30*, 7423.
[28] Y. El Ajjouri, V. S. Chirvony, M. Sessolo, F. Palazon, H. J. Bolink, *RSC Adv.* **2018**, *8*, 41548.
[29] A. D. Jodlowski, A. Yépez, R. Luque, L. Camacho, G. de Miguel, *Angew. Chem., Int. Ed.* **2016**, *55*, 14972.
[30] L. Protesescu, S. Yakunin, O. Nazarenko, D. N. Dirin, M. V. Kovalenko, *ACS Appl. Nano Mater.* **2018**, *1*, 1300.
[31] Y. Liao, C. Song, Y. Xiang, X. Dai, *Ann. Phys.* **2020**, *532*, 2000322.
[32] S. D. Durbin, S. M. Arakelian, Y. R. Shen, *Opt. Lett.* **1981**, *6*, 411.
[33] G. Wang, S. Zhang, X. Zhang, L. Zhang, Y. Cheng, D. Fox, H. Zhang, J. N. Coleman, W. J. Blau, J. Wang, *Photonics Res.* **2015**, *3*, A51.
[34] S. Xiao, B. Lv, L. Wu, M. Zhu, J. He, S. Tao, *Opt. Express* **2015**, *23*, 5875.

[35] X. Li, K. Hu, B. Lyu, J. Zhang, Y. Wang, P. Wang, S. Xiao, Y. Gao, J. He, *J. Phys. Chem. C* **2016**, *120*, 18243.
[36] Y. Wu, Q. Wu, F. Sun, C. Cheng, S. Meng, J. Zhao, R. Merlin, *Proc. Natl. Acad. Sci. U. S. A.* **2015**, *112*, 11800.
[37] W. Wang, Y. Wu, Q. Wu, J. Hua, J. Zhao, *Sci. Rep.* **2016**, *6*, 22072.
[38] R. Wu, Y. Zhang, S. Yan, F. Bian, W. Wang, X. Bai, X. Lu, J. Zhao, E. Wang, *Nano Lett.* **2011**, *11*, 5159.
[39] L. Wu, Y. Dong, J. Zhao, D. Ma, W. Huang, Y. Zhang, Y. Wang, X. Jiang, Y. Xiang, J. Li, Y. Feng, J. Xu, H. Zhang, *Adv. Mater.* **2019**, *31*, 1807981.
[40] J. Zhang, X. Yu, W. Han, B. Lv, X. Li, S. Xiao, Y. Gao, J. He, *Opt. Lett.* **2016**, *41*, 1704.
[41] L. Wu, Z. Xie, L. Lu, J. Zhao, Y. Wang, X. Jiang, Y. Ge, F. Zhang, S. Lu, Z. Guo, J. Liu, Y. Xiang, S. Xu, J. Li, D. Fan, H. Zhang, *Adv. Opt. Mater.* **2018**, *6*, 1700985.
[42] W. Ji, W. Chen, S. Lim, J. Lin, Z. Guo, *Opt. Express* **2006**, *14*, 8958.
[43] L. Lu, X. Tang, R. Cao, L. Wu, Z. Li, G. Jing, B. Dong, S. Lu, Y. Li, Y. Xiang, J. Li, D. Fan, H. Zhang, *Adv. Opt. Mater.* **2017**, *5*, 1700301.
[44] A. B. Villafranca, K. Saravanamuttu, *J. Opt. A: Pure Appl. Opt.* **2009**, *11*, 125202.
[45] B. Shi, L. Miao, Q. Wang, J. Du, P. Tang, J. Liu, C. Zhao, S. Wen, *Appl. Phys. Lett.* **2015**, *107*, 151101.
[46] L. Wu, K. Chen, W. Huang, Z. Lin, J. Zhao, X. Jiang, Y. Ge, F. Zhang, Q. Xiao, Z. Guo, Y. Xiang, J. Li, Q. Bao, H. Zhang, *Adv. Opt. Mater.* **2018**, *6*, 1800400.
[47] J. Li, Z. Zhang, J. Yi, L. Miao, J. Huang, J. Zhang, Y. He, B. Huang, C. Zhao, Y. Zou, S. Wen, *Nanophotonics* **2020**, *9*, 2415.
[48] Y. Shan, L. Wu, Y. Liao, J. Tang, X. Dai, Y. Xiang, *J. Mater. Chem. C* **2019**, *7*, 3811.
[49] M. Bache, F. Eilenberger, S. Minardi, *Opt. Lett.* **2012**, *37*, 4612.
[50] Y. Xu, S. Li, Z. Zhang, Y. Hu, L. Yuan, *Nanotechnology* **2019**, *30*, 295601.
[51] S. Ghosh, S. Paul, S. K. De, *Part. Part. Syst. Charact.* **2018**, *35*, 1800199.
[52] E. López-Fraguas, S. Masi, I. Mora-Seró, *ACS Appl. Energy Mater.* **2019**, *2*, 8381.
[53] B. Saparov, J. P. Sun, W. Meng, Z. Xiao, H. S. Duan, O. Gunawan, D. Shin, I. G. Hill, Y. Yan, D. B. Mitzi, *Chem. Mater.* **2016**, *28*, 2315.
[54] S. Robertson, *Phys. Rev. A* **1979**, *20*, 2170.
[55] W. R. Callen, B. G. Huth, R. H. Pantell, *Appl. Phys. Lett.* **1967**, *11*, 103.
[56] C. M. Nascimento, M. G. A. Silva, *J. Opt. A: Pure Appl. Opt.* **2006**, *8*, 947.
[57] L. Deng, K. He, T. Zhou, C. Li, *J. Opt. A: Pure Appl. Opt.* **2005**, *7*, 409.
[58] R. G. Harrison, L. Dambly, D. Yu, W. Lu, *Opt. Commun.* **1997**, *139*, 69.
[59] L. Lucchetti, S. Suchand, F. Simoni, *J. Opt. A: Pure Appl. Opt.* **2009**, *11*, 034002.
[60] P. Johannisson, D. Anderson, M. Lisak, M. Marklund, *Opt. Commun.* **2003**, *222*, 107.
[61] G. Lifante, *Integrated Photonics : Fundamentals*, Wiley, New York **2002**.
[62] G. C. Valley, M. Segev, B. Crosignani, A. Yariv, M. M. Fejer, M. C. Bashaw, *Phys. Rev. A* **1994**, *50*, R4457.
[63] S. Bian, J. Frejlich, K. H. Ringhofer, *Phys. Rev. Lett.* **1997**, *78*, 4035.
[64] L. Tan, W. A. F. Base, *Chem. Rev.* **2008**, *108*, 1245.
[65] M. D. Dvorak, B. L. Justus, *Opt. Commun.* **1995**, *114*, 147.
[66] K. Wang, Y. Feng, C. Chang, J. Zhan, C. Wang, Q. Zhao, J. N. Coleman, L. Zhang, W. J. Blau, J. Wang, *Nanoscale* **2014**, *6*, 10530.
[67] I. Suárez, H. Gordillo, R. Abargues, S. Albert, J. Martínez-Pastor, *Nanotechnology* **2011**, *22*, 435202.
[68] V. Loriot, P. Béjot, W. Ettoumi, Y. Petit, J. Kasparian, S. Henin, E. Hertz, B. Lavorel, O. Faucher, J.-P. Wolf, *Laser Phys.* **2011**, *21*, 1319.
[69] L. M. Degtyarev, T. P. Lebedeva, *Sov. Phys. JETP* **1984**, *740*, 417.
[70] C. Brée, A. Demircan, G. Steinmeyer, *Opt. Lett.* **2011**, *37*, 1451.
[71] D. L. Weerawarne, X. Gao, A. L. Gaeta, B. Shim, *Phys. Rev. Lett.* **2015**, *114*, 2.
[72] H. A. Ritacco, *Adv. Colloid Interface Sci.* **2017**, *247*, 234.
[73] C. Hosokawa, H. Yoshikawa, H. Masuhara, *Phys. Rev. E: Stat. Phys., Plasmas, Fluids, Relat. Interdiscip. Top.* **2004**, *70*, 7.
[74] P. H. Jones, O. M. MAragó, G. Volpe, *Optical Tweezers. Principles and Applications*, Cambridge University Press, Cambridge **2015**.
[75] M. Sheik-Bahae, A. A. Said, T.-H. Wei, D. J. Hagan, E. W. Van Stryland, *IEEE J. Quantum Electron.* **1990**, *26*, 760.